Probing local spin ordering at surfaces by He^{2+} ions

M. Unipan, A. Robin, D. F. A. Winters,* R. Morgenstern, and R. Hoekstra†
KVI, Atomic Physics, University of Groningen, Zernikelaan 25, NL-9747 AA, Groningen, The Netherlands
(Received 15 August 2006; published 1 December 2006)

Slow, multiply charged ions interacting with surfaces provide a tool for accessing surface properties on a very short length scale. Using characteristic *KLL* Auger electron emission from He^{**} atoms formed in front of a ferromagnetic surface, the local spin polarization of the surface can be linked to the population probability of different spin states in doubly excited He. An atomic model is developed to describe the population of the He^{**} states and their decay. The influences of the surface electronic response and the projectile parameters on the shape of the Auger spectra are discussed. Subsequently, the model is applied to He^{2+} on Ni(110) to extract the surface spin polarization dependence on the crystal temperature from the changes in the relative intensities of Auger peaks corresponding to different spin states. By choosing different scattering conditions, magnetic information on nanometer scale can be obtained.

DOI: 10.1103/PhysRevA.74.062901 PACS number(s): 34.50.Dy, 79.20.Rf, 75.70.−i

I. INTRODUCTION

Ion beams have been extensively used to study the properties of solids and of solid surfaces in particular, owing to the fact that, by carefully choosing the scattering geometry, a well-defined information depth can be obtained [1,2]. Slow ions (with energies of a few tens of eV) interact only with the topmost surface layer within an area of a few (tens of) $Å^2$, offering unique possibilities in accessing two-dimensional (2D) properties. Specifically, the magnetic properties of surfaces have aroused a high interest due to the fact that the reduced dimensionality gives rise to often peculiar behavior, different from the one of the bulk material. For example, ferromagnetic Fe films exhibit antiferromagnetic coupling if separated by Ge spacers of a specific thickness [3], while antiferromagnetic NiO(111) surface spins remain ordered at higher temperatures than in the bulk [4]. Furthermore, highly spin-polarized materials, like half-metallic magnetite, Fe_3O_4, are of great interest to the field of spintronics, where they are used as spin-filter interfaces [5,6]. Techniques that can probe magnetic properties on a very small length scale are required to gain insight into phenomena like antiferromagnetism. Methods used to explore surface magnetism, like spin-polarized metastable atom deexcitation spectroscopy [7], spin-polarized low-energy electron diffraction (SPLEED) [8], or electron capture spectroscopy (ECS) [1,9–12], usually give access to long-range magnetic order.

We developed a method to probe spin polarization at surfaces, called multiple-electron capture spectroscopy (MECS). First results using MECS were presented in earlier works [13,14]. In the present paper we will focus on a detailed description of the model used to analyze and explain the data and recent experimental results will be shown. In MECS, the changes in the characteristic Auger electron emission from doubly excited He atoms are used as a fingerprint of the local surface spin polarization. The He^{**} atoms are formed upon neutralization of He^{2+} ions in front of a surface, in this case ferromagnetic Ni(110), by resonant capture of two electrons from the surface into atomic levels. The neutralization of slow, multiply charged ions in front of surfaces can be described by the classical over-the-barrier (COB) model [15]. According to the COB model, resonant electron capture from the metal becomes possible at a distance where the potential barrier between the solid and ion is lowered to the Fermi level. The electrons are captured into high-lying shells of the projectile, which can subsequently deexcite by autoionization, the emitted Auger electrons producing characteristic spectra [15–19]. While the ion approaches further the surface, an interplay between electron loss to the solid (re-ionization) and electron capture from the surface takes place. The energy distribution of the emitted electrons contains information on the neutralization process and on the electronic structure of the surface [20–22]. For example, the dynamic response of the solid influences the shape of the Auger electron spectra, the peak positions in the *KLL* Auger spectra from He^{**} being shifted to higher energies as compared to emission from gas phase [21]. Also, from the evolution of the spectra with projectile energy, information on the magnitude of the resonant ionization rate can be obtained.

As the spin of the electrons is conserved in the capture process [1,23], there will be different capture probabilities for different spin states if the surface is spin polarized—i.e., majority and minority electrons having different densities of states close to the Fermi level. If the surface has a high degree of spin polarization, it will be more probable to capture electrons into high-spin states (in the case of He, triplet states), while for a low surface polarization, low-spin states (singlet states for He) are favored. When the doubly excited He atoms relax by Auger processes, the relative peak intensities in the *KLL* Auger spectra (corresponding to triplet or singlet states) will change if the surface spin polarization changes, e.g., by changing the temperature of a ferromagnet. As slow He^{2+} ions interact only with an area of a few (tens of) $Å^2$ of the topmost surface layer, MECS has the potential of becoming a useful tool for studying surface magnetism, yielding complementary information to other techniques which can probe magnetism on a scale below the exchange

*Present address: Gesellschaft für Schwerionenforschung (GSI), D-64291 Darmstadt, Germany.
†Electronic address: hoekstra@kvi.nl

TABLE I. Electronic configurations, statistical weights g, binding energies (E_{bin}), Auger electron energies (ε_k), and autoionization rates (Γ_{AI}) [27] for doubly excited $He^{**}(2l2l')$.

State	g	E_{bin} (eV)	ε_k (eV)	Γ_{AI} (10^{14} s^{-1})
$(2s^2)$ ^1S	1	21.13	33.3	1.87
$(2s2p)$ ^3P	9	20.69	33.7	0.12
$(2p^2)$ ^3P	9	19.33		0
$(2p^2)$ ^1D	5	19.12	35.3	0.95
$(2s2p)$ ^1P	3	18.88	35.5	0.54
$(2p^2)$ ^1S	1	16.86	37.3	$\ll$0.01

length, like spin-polarized scannings tunneling microscopy (STM) [24].

II. MULTIPLE-ELECTRON CAPTURE SPECTROSCOPY

A. Experiment

The He^{2+} ions were produced by an electron cyclotron resonance ion source (ECRIS), operated at a potential of 7 kV. After charge-over-mass separation, the ions were guided to our setup by means of a series of magnetic quadrupoles. The ions were decelerated down to energies of a few tens of eV, which was achieved by floating the complete setup on the source potential and applying an additional bias potential V_{bias}. The final kinetic energy of an ion with charge state q is then given by qV_{bias}, plus a small contribution due to the plasma potential of the source of ~8 V [25]. The experiments were performed in a UHV chamber at a pressure of some 10^{-10} mbar. The chamber has μ-metal shielding, in order to prevent stray magnetic fields from disturbing the detection of low-energy electrons. The emitted electrons were detected by a rotatable 180° hemispherical electrostatic analyzer, which has an energy resolution of $\Delta E/E=0.5\%$ and an acceptance of $11.2\times10^{-8}E$ (sr eV) (E being the electron kinetic energy in eV) [25]. As target a ferromagnetic Ni(110) surface was chosen for its expected high-spin polarization at the Fermi edge [26]. The surface of the crystal was cleaned by repeated cycles of sputtering with 20 keV Ar^+ ions and annealing. The sample could be demagnetized by applying an ac magnetic field and by heating up to 700 K. For probing long-range magnetism ECS is used. In ECS the light emitted by deexciting He^* ions is detected and polarization analyzed (this method for probing surface magnetism is described elsewhere; see, e.g., [1,9–12]). A detailed description of our setup can be found in [9].

B. He^{**} states

The He^{**} atoms formed upon He^{2+}-surface interaction can decay by autoionization, giving rise to characteristic *KLL* Auger spectra. The relevant states in doubly excited He, which are the initial states in the autoionization processes, are listed in Table I.

The kinetic energy ε_k of an Auger electron is given by the difference in binding energy E_{bin} between the initial $(2l2l')$ state in He^{**} and the final He^+ $(1s)$ state (which has a binding energy of 54.42 eV). The autoionization (AI) rates listed in Table I are values calculated by Lindroth [27] for free He^{**} atoms. Other calculated [28,29] and experimental [30] AI rates have similar values. For the $(2s2p)$ ^3P state no experimental AI rate is available; only an upper limit of 0.23 $\times10^{14}$ s^{-1} has been determined [30]. The AI rate for the $(2p^2)$ ^3P state is zero because the decay is forbidden, while the AI rate for the $(2p^2)$ ^1S state is very low. Therefore effectively only four states contribute to the *KLL* Auger spectra of helium: namely, $(2s^2)$ ^1S, $(2s2p)$ ^3P, $(2p^2)$ ^1D, and $(2s2p)$ ^1P.

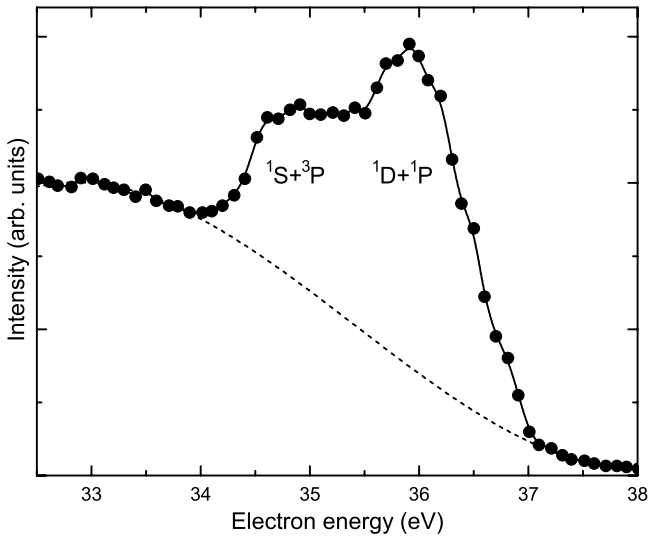

FIG. 1. *KLL* Auger electron spectrum from 20 eV He^{2+} ions incident under 20° on Ni(110).

The statistical weight of each state is given by the spin S and the orbital angular momentum L according to $g=(2S+1)(2L+1)$. Since the states $(2s^2)$ ^1S and $(2s2p)$ ^3P, as well as the $(2p^2)$ ^1D and $(2s2p)$ ^1P states are very close in energy, only two peaks could be resolved experimentally. One corresponds to the pair $(2s^2)$ ^1S, $(2s2p)$ ^3P and is called further the *triplet* peak, whereas the second peak corresponds to the pair $(2p^2)$ ^1D, $(2s2p)$ ^1P and is called further the *singlet* peak. A typical *KLL* Auger spectrum from 20 eV He^{2+} ions incident under 20° on a Ni(110) surface is shown in Fig. 1. The two autoionization peaks sit on top of the high-energy tail of a broad distribution at lower energies, given by electrons originating from Auger deexcitation and Auger neutralization processes [20,21]. This high-energy tail is treated as background to the autoionization signal. The shape of the background is estimated using an algorithm according to Shirley [31] and is represented by the dashed line in Fig. 1.

C. He^{2+} ions impinging on Ni(110)

He^{2+} ions with kinetic energies of 20, 50, or 100 eV were scattered from an unmagnetized Ni(110) surface under 15° incidence, and the emitted *KLL* Auger electrons were detected perpendicular to the ion beam. Figure 2 shows a series of Auger spectra from 20 eV and 50 eV He^{2+} ions, taken for different temperatures of the Ni(110) crystal. The spectra

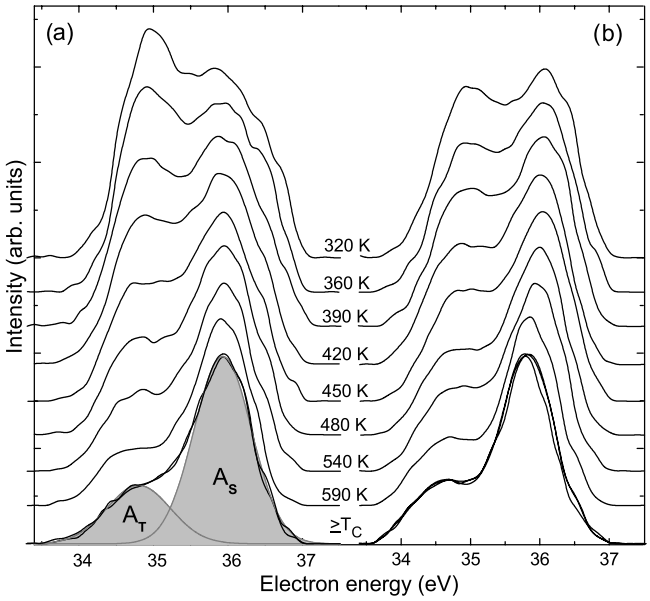

FIG. 2. Normalized *KLL* Auger electron spectra from (a) 20 eV He^{2+} ions and (b) 50 eV He^{2+} ions impinging on Ni(110) under 15° incidence for different temperatures of the crystal.

were background subtracted and normalized to the singlet peak at ~36 eV. A constant offset has been added to the spectra, for clarity. The spectra were fitted with two Gaussians in order to extract the peak intensities A_T and A_S. As the temperature of the Ni(110) crystal is increased, a strong reduction in the intensity of the triplet peak is observed, until the temperature reaches the Curie temperature T_C of Ni of 627 K. The energy position of the triplet peak shifts by ~0.35 eV to lower energies as the temperature increases to T_C, consistent with the suppression of electron capture into the ^3P state, which is higher in energy than the ^1S state by 0.4 eV (see Table I). Above T_C no further changes are observed in the Auger spectra—this is illustrated by spectra taken at 640 K and 660 K which overlap with the one taken at T_C. Spectra were recorded for temperatures up to 50 K above T_C. As the Auger spectra show no more changes above T_C, we can conclude already from the raw spectra that the Curie temperature of the Ni(110) surface coincides with the bulk one, within the experimental uncertainties.

KLL Auger spectra from 100 eV He^{2+} ions (not shown) impinging on Ni(110) under 15° show a similar temperature evolution.

III. FREE-ATOM MODEL

In this section we outline the model which we propose for the description of *KLL* Auger electron spectra from He^{2+} ions scattering off a ferromagnetic surface, in our case a Ni(110) surface. In this so-called "free-atom model," the $(2l2l')$ states in doubly excited He are allowed to decay exponentially like in free atoms and it is assumed that the autoionization rates do not change as the projectile approaches the surface. Besides electron emission by AI, electron loss to the solid by resonant ionization (RI) is also taken into account. The influence of the surface spin polarization on the capture probability for different states in He^{**} is incorporated, which, in turn, influences the shape of *KLL* Auger spectra from He^{**}. In the following, atomic units (a.u.) will be used unless stated otherwise.

Features of the ion-surface interaction in *KLL* Auger spectra from He^{**}

In our model we assume that the He^{**} atoms are formed at a distance in front of the surface where resonant over-the-barrier transitions become possible. According to the classical over-the-barrier model [15], the neutralization distance of He^{+*} is about 8 a.u. Once neutralized, the excited atom will decay by autoionization as it approaches the surface. Close in front of the surface, Auger deexcitation and Auger neutralization become the main deexcitation mechanisms by which the atomic levels are quenched. The presence of the surface strongly perturbs the atomic levels.

The electrons originating from Auger deexcitation or Auger neutralization processes are not taken into account in our model, as they give a broad distribution at lower energies, the higher-energy tail of these electrons being treated as background to the AI signal. Elastically scattered autoionization electrons could end up in the atomic lines, but as only the energy of the electrons is detected as a measure of the initial state from which they originate, the small spin-flip probability [32] of these electrons has no influence on the analysis. The inelastically scattered autoionization electrons will show up at lower energies largely outside the atomic lines.

The atomic levels into which the surface electrons are captured are shifted in energy depending on the ion-surface distance z, owing to the charge—image-charge Coulomb interaction. For the atomic charge an "effective" charge is taken, which accounts for the incomplete screening of the nuclear charge by the electronic cloud. The effective charge is also z dependent. For the doubly excited He atoms the effective charge is taken as $Z_{eff}(z)=2e^{-z/3.5}$, while for He^+ it is taken as $Z_{eff}(z)=1+e^{-z/0.72}$ [21]. The atomic levels shift in energy as $Z_{eff}^2/4z$. The potential curve for an initial $(2l2l')$ state in He^{**} has then a different energy shift as compared to the one for the final He^+ $(1s)$ state.

As the energy difference between the potential energy curves of the initial and final states is z dependent, the energy of the atomic Auger transitions will change as the projectile approaches the surface. In addition, in order to take the dynamic response of the metal into account, the final energy of the autoionization electron $\varepsilon_k(z)$ is taken in between two extreme cases: i.e., the adiabatic and diabatic cases. The adiabatic case corresponds to an infinitely fast rearrangement of the metal electrons, while the diabatic case corresponds to an infinitely slow rearrangement. The ratio between the velocity of the emitted electrons and the Fermi velocity of the metal, $\rho \sim v_a/v_F$, can be regarded as the fastness of the response of the solid to the ionization event. Zeijlmans van Emmichoven *et al.* [21] proposed the following expression for the transition energy:

$$\varepsilon_k(z) = \varepsilon_k^d(z) + [\varepsilon_k^a(z) - \varepsilon_k^d(z)]e^{-\rho/2}, \quad (1)$$

where ε_k^d and ε_k^a are the energies of the autoionization electron for the diabatic and adiabatic cases, respectively. For

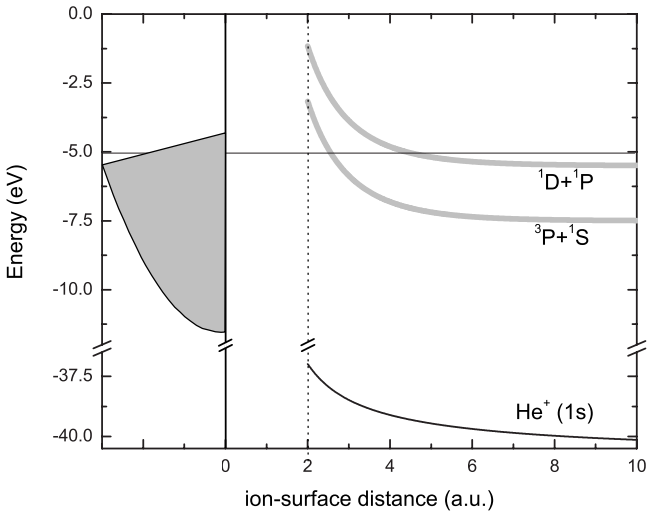

FIG. 3. Atomic-level shifts upon approach to the surface. A schematic kinematically-shifted density of states of the solid is depicted on the left, and the Fermi level is given by the horizontal line.

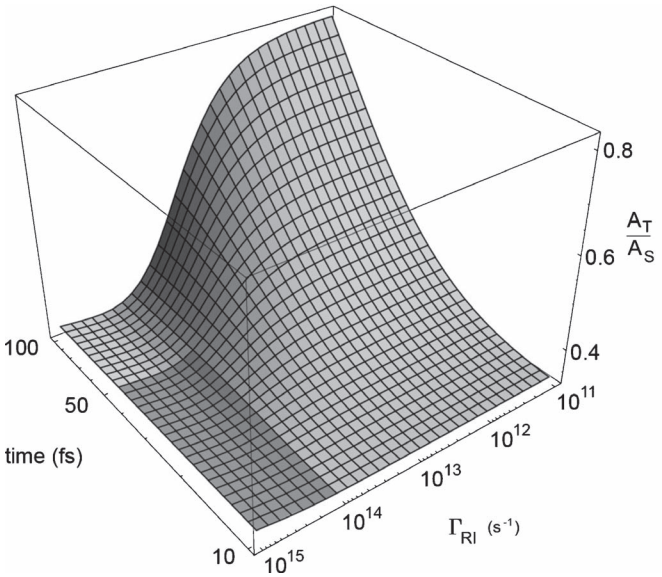

FIG. 4. Triplet-to-singlet peak ratio for an unpolarized surface.

each of the four He** states, in the relevant range of ion-surface distances, the energies ε_k^d and ε_k^a differ by about 0.5 eV.

Figure 3 shows schematically the shift of the atomic levels in doubly excited He relative to the electronic structure of the Ni(110) surface. The density of states (DOS) for Ni(110) is shown here as a modified free-electron metal DOS. This kinematically shifted DOS is the DOS seen in the reference frame of the moving ion [33–35]. The energy scale is relative to the vacuum level. The relevant atomic levels are below the Fermi energy [which is 5.05 eV below vacuum and 9.1 eV above the bottom of the conduction band in the case of Ni(110) [26]] for almost all atom-surface distances. This allows for resonant capture of electrons into these states as soon as the potential barrier between the projectile and surface is low enough. Due to the parallel velocity of the incoming projectile, the electrons of the solid are seen by the ion as having an apparent lower work function, because of the kinematically shifted DOS [33–35]. Therefore electron capture is possible even if the atomic levels are shifted above the "static" Fermi energy.

After resonant electron capture into the He** states, the part of the initial population which has decayed by AI in the time t is given by

$$I_{if}(t) = g_i \Gamma^{if} \tau_i (1 - e^{-t/\tau_i}), \tag{2}$$

where g_i is the statistical weight of the state i, Γ^{if} is the decay rate of the specific $i \rightarrow f$ transition, and $\tau_i = (\Gamma_{AI}^{if} + \Gamma_{RI})^{-1}$ is the lifetime of state i. Decay by resonant ionization was included with an estimated rate of $\Gamma_{RI} = 10^{15}$ s^{-1} [36]. The autoionization rates Γ_{AI}^{if} (taken from Table I) and the resonant ionization rate Γ_{RI} are assumed not to depend on the ion-surface distance z. By summing the decayed fractions $I_{if}(t)$ for the two pairs of states in He**, the triplet-to-singlet intensity ratio A_T/A_S is obtained. For the decay of the He** atoms by AI, only the time between neutralization and quenching of the atomic states at the surface is available [15,21,37]. For our experiments, this time is in the interval 10–50 fs.

In Fig. 4 the triplet-to-singlet peak ratio A_T/A_S is shown as function of the resonant ionization rate and observation time for an unpolarized surface. For resonant ionization rates $>10^{14}$ s^{-1} and observation times in the range 10–50 fs, indicated by the shaded area in Fig. 4, it is expected that the A_T/A_S ratio is rather insensitive to the exact resonant ionization rates and observation times. Experimentally we observed that indeed the A_T/A_S ratio depends only weakly on the observation time (thus on the perpendicular energy of the ion), as shown in Fig. 5.

In order to incorporate the (possible) spin polarization of the surface electrons, the statistical population of the initial states is written as

$$g_i = (2L + 1)\mathcal{P}_{\text{spin}}, \tag{3}$$

where $\mathcal{P}_{\text{spin}}$ is the probability of populating a specific spin system (triplet or singlet) when capturing two electrons. If

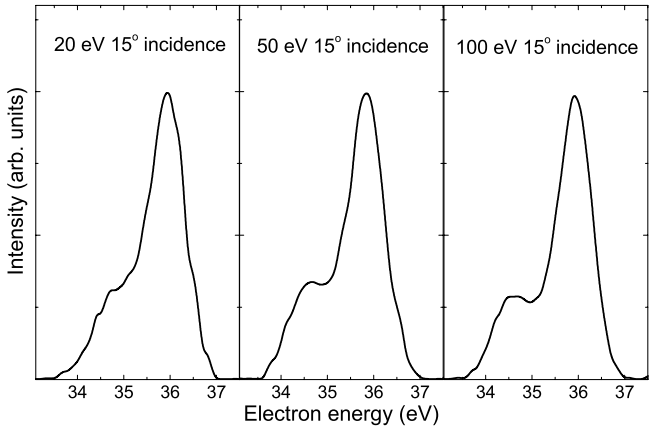

FIG. 5. Normalized *KLL* Auger electron spectra from He^{2+} ions incident on Ni(110) for a crystal temperature of 650 K.

we write the spin polarization of the surface as

$$P = \frac{n_\uparrow - n_\downarrow}{n_\uparrow + n_\downarrow}, \tag{4}$$

with $n_\uparrow$ and $n_\downarrow$ the fractions of spin-up and spin-down electrons, respectively ($n_\uparrow + n_\downarrow = 1$), then the probabilities to capture two electrons into either a triplet or a singlet state are

$$\mathcal{P}_t = n_\uparrow n_\uparrow + n_\downarrow n_\downarrow + n_\uparrow n_\downarrow,$$

$$\mathcal{P}_s = n_\uparrow n_\downarrow. \tag{5}$$

From Eqs. (4) and (5) it follows that

$$\mathcal{P}_t = \frac{3 + P^2}{4},$$

$$\mathcal{P}_s = \frac{1 - P^2}{4}. \tag{6}$$

For zero polarization one finds the statistical 3:1 ratio between triplet and singlet states.

With the above ingredients *KLL* Auger spectra from He^{**} can be simulated using a Monte Carlo method in the following manner: we include the statistical population of states from Eqs. (3) and (6) in the expression for the fractions decayed by AI [Eq. (2)]. Then the atoms are allowed to decay along their trajectory by emitting an Auger electron at any random distance z between the neutralization distance z_{neut} and a distance above the surface where the quenching of the atomic states takes place ($\approx$2 a.u.). The energy of the emitted electrons will depend on z, as the difference between the initial- and final-state potential curves is dependent on z.

The decayed fractions I_{if} are then convoluted with a Gaussian spectrometer function [full width at half maximum (FWHM)=0.75 eV]. A series of calculated spectra is shown in Fig. 6 for 20 eV He^{2+} impinging on a Ni(110) surface for different degrees of surface spin polarization (a constant offset has been added to the spectra, for clarity). The evolution of the calculated spectra is very similar to the measured spectra from Fig. 2. Using the same value of the parameter ρ in Eq. (1) as in [21], the energy of the Auger peaks shifts to higher energies compared to the case of emission from atoms in the gas phase (from $\simeq$33.5 eV to $\simeq$34.4 eV for the triplet peak and from $\simeq$35.4 eV to $\simeq$36 eV for the singlet peak), while the spacing between the peaks decreases. This result reproduces quite well the peak shifts observed experimentally.

The intensity ratio of the triplet and singlet peaks in the *KLL* spectra depends on the surface spin polarization and can be expressed as follows:

$$\frac{A_T}{A_S} = \frac{I_{^1S} + I_{^3P}}{I_{^1D} + I_{^1P}} = c_S + c_T \frac{3 + P^2}{1 - P^2}, \tag{7}$$

with the coefficients c_S and c_T given by

$$c_S = \left. \frac{I_{^1S}}{I_{^1D} + I_{^1P}} \right|_{P=0},$$

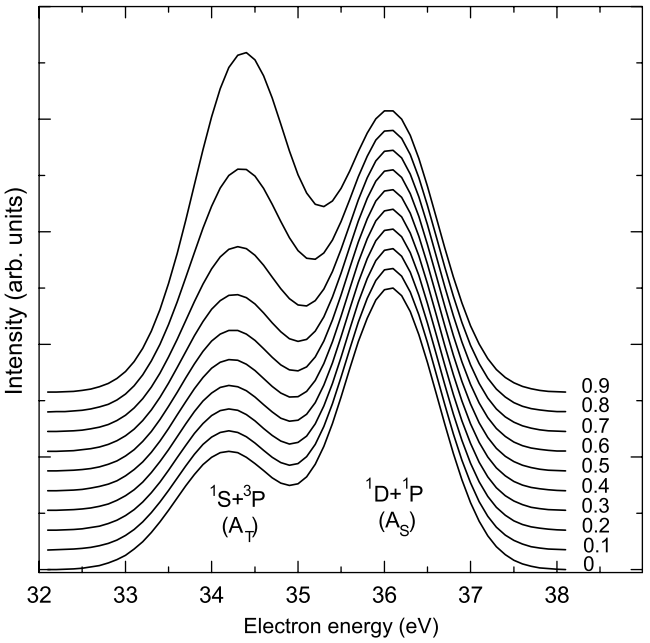

FIG. 6. Calculated spectra for 20 eV He^{2+} on Ni(110) under 15° incidence for different degrees of polarization of the target, indicated on the right. The spectra are normalized to the higher-energy (singlet) peak.

$$3c_T = \left. \frac{I_{^3P}}{I_{^1D} + I_{^1P}} \right|_{P=0}. \tag{8}$$

The sum of c_S and c_T gives the triplet-to-singlet ratio for an unpolarized surface, in our case for temperatures of the crystal above Curie temperature T_C,

$$\left. \frac{A_T}{A_S} \right|_{T \geq T_C} = c_S + 3c_T, \tag{9}$$

with values in the interval 0.34–0.39, for the observation times of our experiments. These values for the A_T/A_S ratio are very close to the ones we observed experimentally. As the spin polarization of the surface increases, so does the probability of capturing two electrons into triplet states, leading to an increase in the relative intensity of the triplet peak. Therefore, the triplet-to-singlet peak ratio can be used as a measure of the surface spin polarization.

IV. RESULTS AND DISCUSSION

The exchange interaction in a magnetic surface is weakened by the loss of magnetic neighbors, leading to a faster thermal decrease of the spin order. In models treating the temperature dependence of the surface spin polarization, two temperature ranges are described separately: the critical limit, for temperatures close to the Curie temperature T_C, and the low-temperature limit. For temperatures well below T_C, in the regime of spin-wave models, the surface magnetization is expected to follow, like the bulk, the Bloch law ($1 - bT^{3/2}$), but with the coefficient b enhanced 2–3 times for the surface as compared to bulk [38,39]. The critical behav-

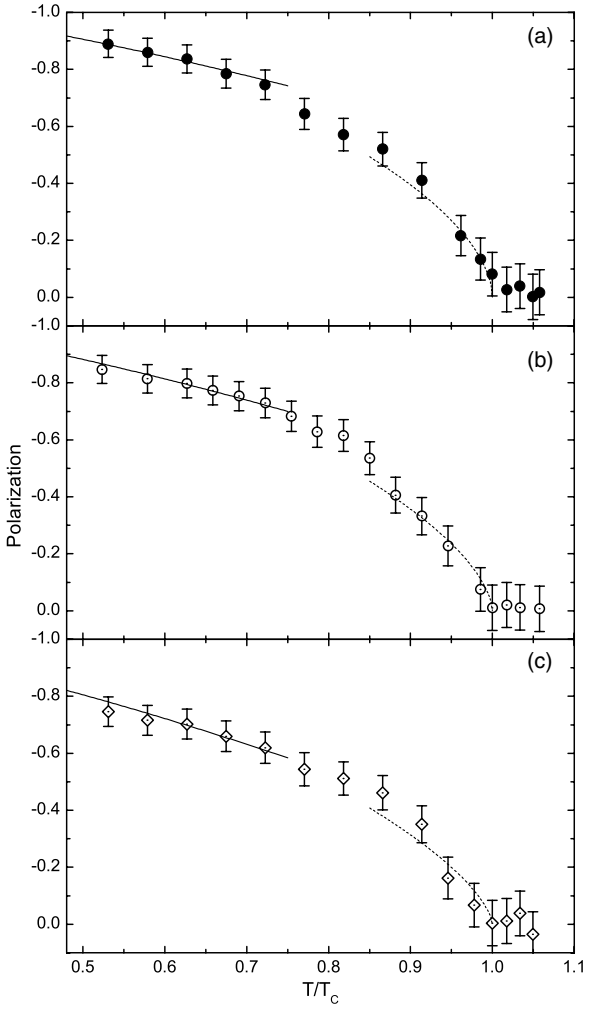

FIG. 7. Dependence of the surface spin polarization on the Ni(110) temperature for (a) 20 eV, (b) 50 eV, and (c) 100 eV, 15° incidence He^{2+} ions. The solid curves are fits with a $(1-bT^{3/2})$ dependence. The dashed curves are fits with a $(1-T/T_C)^{\beta}$ dependence.

ior near T_C is governed by a $(1-T/T_C)^{\beta}$ law, with the critical exponent $\beta \simeq 0.7-0.8$ for surfaces, as compared to $\beta=1/3$ for bulk ferromagnets [40].

A. Temperature dependence of the Ni(110) surface spin polarization

Knowing the A_T/A_S peak ratio for every temperature point and calculating c_S and c_T for every specific ion energy, Eq. (7) can be solved for P. In this way, the temperature dependence of the spin polarization can be determined. The results of this procedure are shown in Fig. 7 for the three projectile energies that we have used. As the peak ratio has a quadratic dependence on the surface spin polarization [Eq. (7)], the sign of the polarization needs to be determined independently. We used ECS on magnetized Ni(110)[9] and found a negative surface spin polarization for Ni(110).

For all three projectile energies, two regimes can be clearly identified in the polarization temperature dependence. In the temperature range close to T_C, the polarization seems to follow a critical behavior with an exponent $\beta \simeq 0.65$ (0.61 ± 0.14 for 20 eV, 0.65 ± 0.11 for 50 eV, and 0.69 ± 0.15 for 100 eV ions). The values of β we obtained are reasonably close to $\beta=0.76$ determined from SPLEED measurements, with high-temperature resolution, by Alvarado *et al.* [41]. For temperatures lower than $0.7T_C$, a different dependence is evident. Although the temperature range of our measurements does not extend to temperatures low enough for the Bloch-law behavior to be fully valid, we attempted to fit a $T^{3/2}$ law to the surface polarization in the range $(0.5-0.7)T_C$, as shown by the solid lines in Fig. 7. The coefficients b obtained from this fit are $(1.9\pm0.5)\times10^{-5}$ $K^{-3/2}$, $(2.1\pm0.4)\times10^{-5}$ $K^{-3/2}$, and $(2.3\pm0.5)\times10^{-5}$ $K^{-3/2}$ for 20, 50, and 100 eV He^{2+} ions, respectively. These values are approximately 3 times larger than the one measured for bulk Ni—i.e., 7.5×10^{-6} $K^{-3/2}$ [42]—in accordance with the expected enhancement at the surface.

At room temperature ($\simeq 0.5T/T_C$), the polarization as obtained with 20 eV, 15° incidence He^{2+} ions is close to −90%, in agreement with previous theoretical and experimental results [26,43]. We have to point out that this MECS value is the spin polarization of the electrons close to the Fermi level, as they are the ones (resonantly) captured into atomic levels. Other techniques for probing the spin polarization (like spin-polarized metastable deexcitation spectroscopy [7] or field emission electron spectroscopy [44]) deal with the polarization of electrons coming from a wider part of the band structure and the obtained values of the polarization are then different. Furthermore, in these latter cases electron tunneling is involved and the (very) different tunneling probabilities for s and p, on the one hand, and d electrons, on the other hand, have to be considered.

Apparently, for 50 and 100 eV, 15° incidence He^{2+} ions, the polarization obtained at room temperature is lower than for 20 eV (cf. Fig. 7). The lower spin polarization observed for 50 and 100 eV He^{2+} ions could indicate that the captured electrons have a weaker spin coupling. The changes in the observed polarization are not likely to be caused by a variation of the electron polarization perpendicular to the surface, as trajectory simulations using the KALYPSO 2 code [45] indicated that the turning point of the ions trajectory is the same for all ion energies used here (about 2 a.u. above the surface). The lowering of the polarization with increasing projectile energy can be understood if we bear in mind that the spin correlation length in Ni is in the order of ≃20 a.u. [46,47]. According to COB, the distance along the surface between the first and second electron capture for He^{2+} ions varies from ~3 a.u. for 20 eV, 20° incidence to ~10 a.u. for 100 eV, 20° incidence. The difference in distances along the surface is mainly caused by the image-charge interaction, which causes an energy gain perpendicular to the surface of ≈3 eV for He^{2+} and leading to a larger effective incidence angle of the projectile. The lower the energy of the ion is, the larger the effective angle, because of the increased relative importance of the image-charge energy gain. In Fig. 8 is shown the room-temperature (RT) polarization, obtained by MECS, as a function of the distance along the surface between the first and second electron capture, ξ. The data points were obtained from results using different He^{2+} energies and incidence angles (the solid curve is to guide the

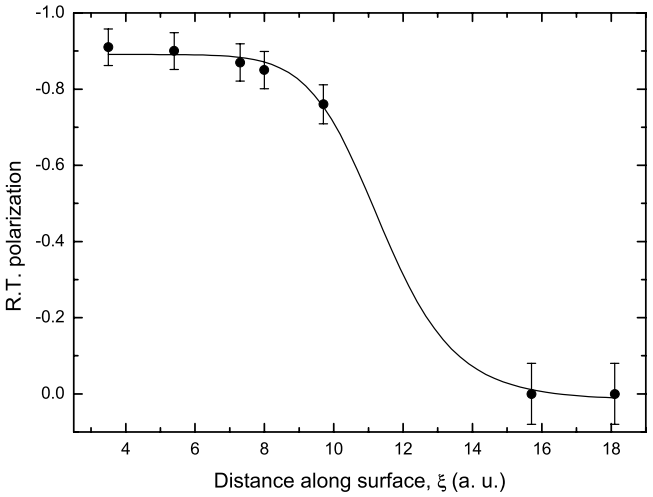

FIG. 8. RT polarization of Ni(110) from MECS as function of the distance along the surface between the first and second electron capture (according to COB model).

eye). The measured RT polarization shows a decreasing trend with increasing ξ, and most striking, for grazing incidence the polarization vanishes. The distance along the surface between the first and second electron capture is, of course, a crude approximation of the effective area where the He^{2+} ions capture electrons from. Nevertheless, Fig. 8 can give a fair idea of the scale of the spin correlation length, which seems to be about 16 a.u.. Furthermore, it is of interest to investigate temperature-dependent $P(\xi)$ curves, which would allow one to obtain the correlation length evolution with temperature.

B. Total intensity change in *KLL* Auger spectra from He^{**}

So far we have focused on the relative change in the intensity of the triplet peak; the advantage of using the A_T/A_S as the measured quantity is the cancellation of possible long-term fluctuations in the ion beam current (due to thermal drifts and plasma instabilities in the ion source). The intensity of the singlet peak should decrease with increasing surface polarization (thus with decreasing surface temperature), as the weight of the capture probability shifts to the ^3P state. This implies that the total intensity of the emitted autoionization electrons should decrease with increasing surface spin polarization, because, as the capture in the ^3P state becomes more important, so does the electron loss via resonant ionization [due to the smaller branching ratio $\Gamma_{AI}^{3P}/(\Gamma_{AI}^{3P}+\Gamma_{RI})$ of the ^3P state compared to the singlet states]. These effects are illustrated in Fig. 9, where the series of spectra as in Fig. 2(a) is shown, but this time not normalized.

In Fig. 9 it can be seen that the decrease of the triplet peak is concurrent with the increase of the singlet peak, as the temperature of the Ni(110) crystal increases. By integrating the spectra over the whole energy range of interest, the total intensity is obtained. Using the polarization dependences on temperature (Fig. 7), the total intensity can be plotted as a function of the surface polarization and is shown in Fig. 10. The curves are the calculated total intensities from the free-

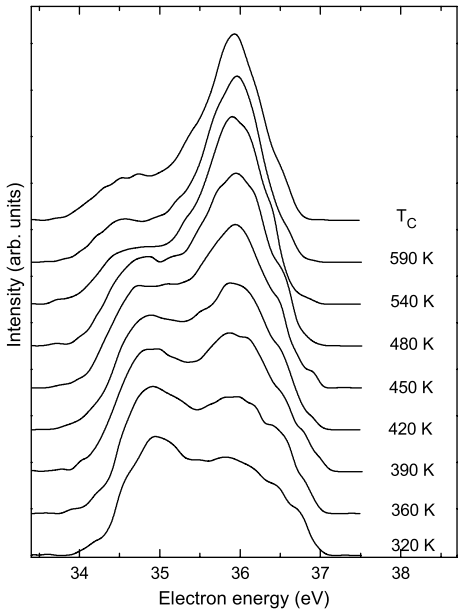

FIG. 9. Same as Fig. 2, but not normalized, *KLL* Auger electron spectra from 20 eV He^{2+} on Ni(110) under 15° incidence (a constant offset is added for clarity).

atom model for the three projectile energies that we have used.

All series have been normalized to the intensity value at T_C, which corresponds to zero polarization. The calculated total intensity dependence on polarization was obtained by summing the decayed fractions corresponding to the four states contributing to the *KLL* Auger spectra for each of the three scattering conditions. The atomic model describes the data fairly well, especially the increasing trend with temperature. For a better agreement, the variation of the decay rates with the ion-surface distance should be included in the model, as they are strongly influencing the total electron

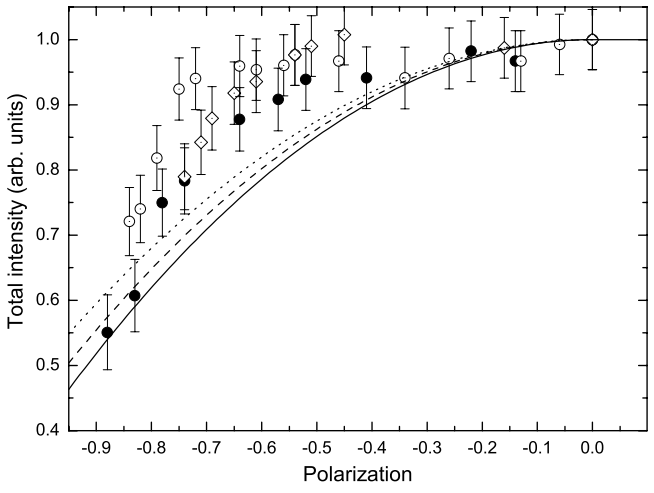

FIG. 10. Polarization dependence of the total intensity of autoionization electrons from 20 eV (●), 50 eV (○), and 100 eV (◇), 15° incidence He^{2+} ions on Ni(110). The curves are the calculated intensities for 20 eV (solid line), 50 eV (dashed line), and 100 eV (dotted line) He^{2+} ions.

emission. But the problem of Auger transition rates in front of metallic surfaces is not straightforward, and accurate theoretical and/or experimental data are needed. Promising results were obtained by Wethekam and Winter [48] on the Auger neutralization of He^+ ions in front of metallic surfaces. When considering peak intensity ratios, though, it is reasonable to assume that the changes in the autoionization rates follow the same behavior for the four $(2l2l')$ states in He^{**} and are therefore canceled out. Another point of improvement in the model could be the inclusion of the different emission anisotropy of the $(2l2l')$ states in doubly excited He.

V. CONCLUSION

An atomic model was developed in order to explain and analyze the shape of the autoionization spectra from doubly excited He atoms formed in front of a ferromagnetic Ni(110) surface. By introducing electron capture probabilities for different spin states—i.e., capture probabilities dependent on the number of available majority and minority electrons close to the Fermi level—the changes in the relative peak intensities observed in the *KLL* Auger spectra can be linked to the surface spin polarization. In this way, the temperature dependence of the spin polarization of the Ni(110) surface can be extracted from the temperature evolution of the Auger spectra.

Combining spin polarization data from different scattering conditions with information on the ionic trajectories indicates that MECS can be used to obtain information on magnetism at the electron exchange length scale, too. In this respect, MECS might become a complementary tool for investigating magnetic phenomena of reduced dimensionality on subnanometer length scales, like antiferromagnetism or magnetism of nanostructures and thin films.

ACKNOWLEDGMENTS

We gratefully acknowledge the support of the KVI technical staff. This work is part of the research programme of the Stichting voor Fundamenteel Onderzoek der Materie (FOM), which is financially supported by the Stichting voor Nederlands Wetenschappelijk Onderzoek (NWO), and of the research collaboration agreement of the Gesellschaft für Schwerionenforschung (GSI) and the Rijksuniversiteit Groningen (RuG). A.R. acknowledges support from the European Union (EU) within the HITRAP project (Contract No. HPRI-CT-2001-50036).

[1] H. Winter, Phys. Rep. **367**, 387 (2002).
[2] H. Niehus, W. Heiland, and E. Taglauer, Surf. Sci. Rep. **17**, 213 (1993).
[3] P. Walser, M. Schleberger, P. Fuchs, and M. Landolt, Phys. Rev. Lett. **80**, 2217 (1998).
[4] A. Barbier *et al.*, Phys. Rev. Lett. **93**, 257208 (2004).
[5] Yu. S. Dedkov, U. Rüdiger, and G. Güntherodt, Phys. Rev. B **65**, 064417 (2002).
[6] N. Berdunov, S. Murphy, G. Mariotto, and I. V. Shvets, Phys. Rev. Lett. **93**, 057201 (2004).
[7] M. Onellion, M. W. Hart, F. B. Dunning, and G. K. Walters, Phys. Rev. Lett. **52**, 380 (1984).
[8] F. B. Dunning and G. K. Walters, in *Spin Polarized Electrons in Surface Physics*, edited by R. Feder (World Scientific, Singapore, 1985).
[9] M. Unipan, D. F. A. Winters, A. Robin, R. Morgenstern, and R. Hoekstra, Nucl. Instrum. Methods Phys. Res. B **230**, 356 (2005).
[10] J. Manske, M. Dirska, G. Lubinski, M. Schleberger, A. Närmann, and R. Hoekstra, J. Magn. Magn. Mater. **168**, 249 (1997).
[11] J. Leuker, H. W. Ortjohann, R. Zimny, and H. Winter, Surf. Sci. **388**, 262 (1997).
[12] M. Gruyters, T. Bernhard, and H. Winter, Phys. Rev. Lett. **94**, 227205 (2005).
[13] M. Unipan, A. Robin, R. Morgenstern, and R. Hoekstra, Phys. Rev. Lett. **96**, 177601 (2006).
[14] M. Unipan, A. Robin, D. F. A. Winters, R. Morgenstern, and R. Hoekstra, Nucl. Instrum. Methods Phys. Res. B **232**, 1 (2005).
[15] J. Burgdörfer, P. Lerner, and F. W. Meyer, Phys. Rev. A **44**, 5674 (1991).
[16] J. Limburg, J. Das, S. Schippers, R. Hoekstra, and R. Morgenstern, Phys. Rev. Lett. **73**, 786 (1994).
[17] F. W. Meyer, S. H. Overbury, C. C. Havener, P. A. Zeijlmans van Emmichoven, J. Burgdörfer, and D. M. Zehner, Phys. Rev. A **44**, 7214 (1991).
[18] N. Stolterfoht *et al.*, Phys. Rev. A **52**, 445 (1995).
[19] H. P. Winter and F. Aumayr, J. Phys. B **32**, R39 (1999).
[20] H. D. Hagstrum and G. E. Becker, Phys. Rev. B **8**, 107 (1973).
[21] P. A. Zeijlmans van Emmichoven, P. A. A. F. Wouters, and A. Niehaus, Surf. Sci. **195**, 115 (1988).
[22] H. Khemliche, T. Schlathölter, R. Hoekstra, R. Morgenstern, and S. Schippers, Phys. Rev. Lett. **81**, 1219 (1998).
[23] R. Pfandzelter, T. Bernhard, and H. Winter, Phys. Rev. Lett. **86**, 4152 (2001).
[24] R. Wiesendanger *et al.*, J. Magn. Magn. Mater. **272-276**, 2115 (2004).
[25] S. T. deZwart, A. G. Drentje, A. L. Boers, and R. Morgenstern, Surf. Sci. **217**, 298 (1989).
[26] F. Mittendorfer, A. Eichler, and J. Hafner, Surf. Sci. **423**, 1 (1999).
[27] E. Lindroth, Phys. Rev. A **49**, 4473 (1994).
[28] Y. K. Ho and A. K. Bhatia, Phys. Rev. A **44**, 2895 (1991).
[29] D. H. Oza, Phys. Rev. A **33**, 824 (1986).
[30] P. J. Hicks and J. Comer, J. Phys. B **8**, 1866 (1975).
[31] D. A. Shirley, Phys. Rev. B **5**, 4709 (1972).
[32] D. L. Abraham and H. Hopster, Phys. Rev. Lett. **59**, 2333 (1987).
[33] H. Winter, Nucl. Instrum. Methods Phys. Res. B **78**, 38 (1993).
[34] R. Zimny and Z. L. Mišković, Nucl. Instrum. Methods Phys. Res. B **58**, 387 (1991).

[35] J. Los and J. J. C. Geerlings, Phys. Rep. **190**, 133 (1990).
[36] W. Sesselmann *et al.*, Phys. Rev. B **35**, 1547 (1987).
[37] S. Schippers, J. Limburg, J. Das, R. Hoekstra, and R. Morgenstern, Phys. Rev. A **50**, 540 (1994).
[38] G. T. Rado, Bull. Am. Phys. Soc. **2**, 127 (1957).
[39] M. Taborelli, O. Paul, O. Züger, and M. Landolt, J. Phys. (Paris), Colloq. **49**, C8-1659 (1988).
[40] K. Binder, in *Spin Polarized Electrons in Surface Physics*, edited by R. Feder (World Scientific, Singapore, 1985).
[41] S. F. Alvarado, M. Campagna, F. Ciccacci, and H. Hopster, J. Appl. Phys. **53**, 7920 (1982).
[42] B. E. Argyle, S. H. Charap, and E. W. Pugh, Phys. Rev. **132**, 2051 (1963).
[43] E. Kisker, W. Gudat, E. Kuhlmann, R. Clauberg, and M. Campagna, Phys. Rev. Lett. **45**, 2053 (1980).
[44] M. Landolt and M. Campagna, Surf. Sci. **70**, 197 (1978).
[45] M. A. Karolewski, Nucl. Instrum. Methods Phys. Res. B **230**, 402 (2005).
[46] F. Huang, G. J. Mankey, M. T. Kief, and R. F. Willis, J. Appl. Phys. **73**, 6760 (1993).
[47] L. Sun, P. C. Searson, and C. L. Chien, Phys. Rev. B **61**, R6463 (2000).
[48] S. Wethekam and H. Winter, Phys. Rev. Lett. **96**, 207601 (2006).